

Valence bond solid and possible deconfined quantum criticality in an extended kagome lattice Heisenberg antiferromagnet

Alexander Wietek^{1,*} and Andreas M. Läuchli²

¹Center for Computational Quantum Physics, Flatiron Institute, 162 5th Avenue, NY 10010, New York, USA

²Institut für Theoretische Physik, Universität Innsbruck, A-6020 Innsbruck, Austria

(Dated: December 10, 2021)

We present numerical evidence for the emergence of an extended valence bond solid (VBS) phase at $T = 0$ in the kagome $S = 1/2$ Heisenberg antiferromagnet with ferromagnetic further-neighbor interactions. The VBS is located at the boundary between two magnetically ordered regions and extends close to the nearest-neighbor Heisenberg point. It exhibits a diamond-like singlet covering pattern with a 12-site unit-cell. Our results suggest the possibility of a direct, possibly continuous, quantum phase transition from the neighboring $\mathbf{q} = 0$ coplanar magnetically ordered phase into the VBS phase. Moreover, a second phase which breaks lattice symmetries, and is of likely spin-nematic type, is found close to the transition to the ferromagnetic phase. The results have been obtained using numerical Exact Diagonalization. We discuss implications of our results on the nature of nearest-neighbor Heisenberg antiferromagnet.

Introduction — We expect the unexpected when strong electron interactions meet geometric frustration. The emergence of novel exotic states of matter in frustrated quantum magnets is intensely studied in experiments, theory, and numerical computations. Several materials and theoretical models exhibit a lack of magnetic ordering even at lowest temperatures. Instead, genuine quantum many-body states, like quantum spin liquids [1, 2] or valence bond solids (VBS) can be observed [3–6].

The nearest-neighbor kagome lattice Heisenberg spin 1/2 antiferromagnet arguably remains one of the most puzzling conundrums in frustrated magnetism. Various scenarios on the nature of its ground state have been proposed. It has been found early, that a VBS is energetically competitive [7–11]. However, more recent numerical studies suggest, that different spin disordered states are a more likely scenario. Several density-matrix renormalization group (DMRG) studies later suggested the possibility of a gapped spin liquid ground state [12, 13]. More recently, variational Monte Carlo and tensor network studies also suggested a gapless spin liquid state being realized [14–18]. While conclusion on the nature of its ground state has not unanimously been reached to date [19], several exotic new states of matter have been clearly identified in close proximity to the nearest-neighbor model [20–23]. Among those, a chiral spin liquid has been found in an extended Heisenberg model with antiferromagnetic second and third nearest-neighbor interactions [21–23]. The classical ground state phase diagram of this model has previously been established [24, 25]. A phase transition between two magnetic orders has been found for antiferromagnetic interactions. In the quantum case, the chiral spin liquid phase is located at the transition line between these two magnetic phases and extends close to the nearest-neighbor point. The classical phase diagram also contains a phase transition line between two types of coplanar magnetic orders for *ferromagnetic* second and third nearest-neighbor interactions. Given that some frustrated kagome materials involving both ferromagnetic and antiferromagnetic couplings are known to exist [26, 27], there is a strong interest to explore whether novel

phases also emerge at or in the vicinity of the classical transition line at $J_3 = 2J_2 < 0$.

Here, we investigate the kagome spin 1/2 Heisenberg antiferromagnet with additional ferromagnetic second and third nearest-neighbor interactions. We present conclusive numerical evidence for the appearance of a *diamond* VBS phase in an extended parameter range. The VBS phase is located in the vicinity of the classical transition line between the $\mathbf{q} = 0$ and $\sqrt{3} \times \sqrt{3}$ magnetic orders. Interestingly, the phase extends close up to the nearest-neighbor Heisenberg point.

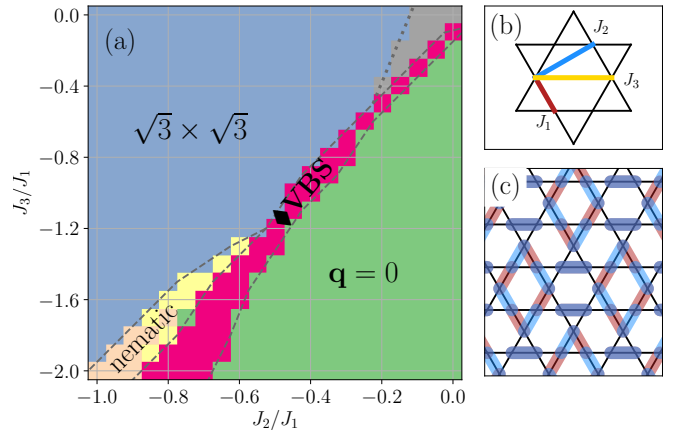


FIG. 1. (a) Approximate phase diagram of the extended kagome Heisenberg model Eq. (1) for $J_1 > 0$ and $J_2, J_3 \leq 0$ as obtained from ED on a 36-site simulation cluster. Between two regions of magnetic $\mathbf{q} = 0$ and $\sqrt{3} \times \sqrt{3}$ order a diamond VBS and a spin nematic phase are emerging. Different colors denote the quantum numbers of the first excited state. Green: $S = 1$, $\Gamma.D6.A2$ or $\Gamma.D6.E2$. Blue: $S = 1$, $\Gamma.D6.B1$ or $K.D3.A1$. Pink: $S = 0$, $M.D2.A2$. Orange: $S = 0$, $M.D2.A1$. Yellow: $S = 2$, $\Gamma.D6.A1$. Gray: $S = 0$, various space group sectors. Gray lines are a guide to the eye. (b) Coupling geometry for the Hamiltonian Eq. (1). (c) Structure of the diamond VBS with a 12-site unit cell. Dimer coverings on the diamond structure are in resonance.

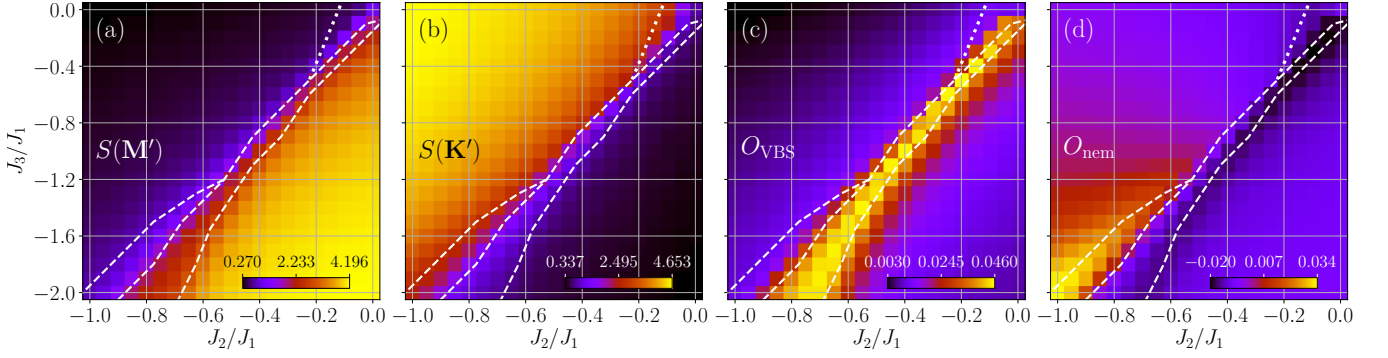


FIG. 2. (a) Spin structure factor $S(\mathbf{M}')$ evaluated at $\mathbf{M}' = (2\pi, 2\pi/\sqrt{3})$, indicating $\mathbf{q} = 0$ magnetic order. (b) Spin structure factor $S(\mathbf{K}')$ evaluated at $\mathbf{K}' = (8\pi/3, 0)$, indicating $\sqrt{3} \times \sqrt{3}$ magnetic order. (c) Diamond VBS order parameter O_{VBS} as defined in Eq. (6). A diamond VBS phase is emerging in between the two magnetic orders. (d) Nematic phase order parameter O_{nem} as defined in Eq. (7), indicating the extent of the plaquette-nematic phase. Note the good agreement between the order parameter inferred phase diagram and the excited state spectroscopy phase diagram of Fig. 1 indicated with the dashed white lines.

Model and phase diagram — We consider the Hamiltonian,

$$H = J_1 \sum_{\langle i,j \rangle} \vec{S}_i \cdot \vec{S}_j + J_2 \sum_{\langle\langle i,j \rangle\rangle} \vec{S}_i \cdot \vec{S}_j + J_3 \sum_{\langle\langle\langle i,j \rangle\rangle\rangle_h} \vec{S}_i \cdot \vec{S}_j, \quad (1)$$

on a kagome lattice geometry, where $\vec{S}_i = (S_i^x, S_i^y, S_i^z)$ denotes spin 1/2 operators, $\langle \dots \rangle$ and $\langle\langle \dots \rangle\rangle$ denotes the sum over nearest- and second nearest-neighbor sites, and $\langle\langle\langle \dots \rangle\rangle\rangle_h$ denotes sum over third nearest-neighbor interactions only across the hexagons of the kagome lattice, cf. Fig. 1(b). In the following, we set $J_1 = 1$ and focus on the case of ferromagnetic couplings $J_2 < 0$ and $J_3 < 0$.

Our results are obtained by Exact Diagonalization (ED) calculations on a $N = 36$ site kagome lattice with periodic boundary conditions [28]. Its Brillouin zone features the \mathbf{K} and \mathbf{M} points and is hence suited to stabilize both the $\sqrt{3} \times \sqrt{3}$ and $\mathbf{q} = 0$ order. We detect ordering by investigating suitably chosen order parameters and performing tower-of-states analysis, i.e. comparing quantum numbers of finite-size energy eigenstates with theoretical predictions. The order parameters of the ground state and finite-size energy spectra are calculated on a grid for $J_2 \in [-1, 0]$ with spacing 0.05 and $J_3 \in [-2, 0]$ with spacing 0.1.

For classical Heisenberg spins the phase diagram of this model has been established in Ref. [25]. The $\sqrt{3} \times \sqrt{3}$ magnetic phase is separated from the $\mathbf{q} = 0$ magnetic phase by a critical line located at $J_3 = 2J_2$. For $J_3 < -2$ and $J_2 < -1$ a ferromagnetic state is stabilized.

In Fig. 1 we present a first exploration of the quantum ($S = 1/2$) phase diagram based on a map organized by the quantum numbers of the first excitation above the ground state. The assignment of the phases is performed based on a tower-of-states analysis for different candidate phases. According to this rationale, the blue region indicates the $\sqrt{3} \times \sqrt{3}$ magnetic order, the green region indicates the $\mathbf{q} = 0$ magnetic

order and the pink region the VBS phase. The nematic phase extends in the yellow and orange region, where two different quantum numbers are the first excitation. The gray lines serve as a guide to the eye and determine approximate phase boundaries. Apart from the expected $\sqrt{3} \times \sqrt{3}$ and $\mathbf{q} = 0$ coplanar magnetic order phases, we find an unanticipated diamond VBS and a lattice symmetry breaking spin nematic phase located in the vicinity of the classical transition line. In Fig. 2 we corroborate the spectroscopy picture with an analysis of corresponding order parameters. The spin nematic phase extends close to the classical ferromagnetic phase, while the VBS phase extends close to the nearest-neighbor point. We now proceed to characterize the reported phases in more detail.

Magnetic order — The $\mathbf{q} = 0$ and $\sqrt{3} \times \sqrt{3}$ magnetic phases break spin rotational $\text{SU}(2)$ symmetry and exhibit patterns of magnetic ordering shown in the supplementary material [29]. We consider the static spin structure factor,

$$S(\mathbf{q}) = \frac{1}{N} \sum_{k,l=1}^N e^{-i\mathbf{q} \cdot (\mathbf{r}_k - \mathbf{r}_l)} \langle \vec{S}_k \cdot \vec{S}_l \rangle. \quad (2)$$

For the two magnetic orders, the structure factor is peaked at the points

$$\mathbf{M}' = (2\pi, 2\pi/\sqrt{3}) \quad \text{for } \mathbf{q} = 0 \text{ order}, \quad (3)$$

$$\mathbf{K}' = (8\pi/3, 0) \quad \text{for } \sqrt{3} \times \sqrt{3} \text{ order}, \quad (4)$$

in the extended Brillouin zone, cf. [24]. Hence, $S(\mathbf{M}')$ and $S(\mathbf{K}')$ shown in Fig. 2(a) and (b) identify both magnetic phases, respectively. The regions where these structure factors are peaked coincide with the blue and green regions in Fig. 1. The blue region in Fig. 1(a) is given by the points, where the first excitation is a triplet, $S = 1$, state with K.D3.A1 or $\Gamma.\text{D6.B1}$ space group quantum numbers [29, 30]. In the green region in Fig. 1(a), the triplet states, $S = 1$, with $\Gamma.\text{D6.A2}$ and $\Gamma.\text{D6.E2}$ space group quantum numbers are the first excitation. Thus, the spin structure factor and energy spectroscopy yield consistent results on the extent of these two phases.

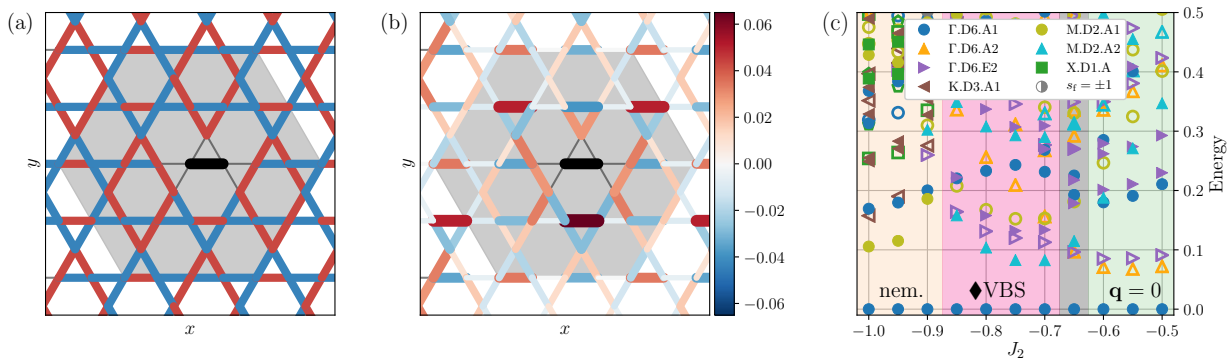


FIG. 3. Diamond VBS: (a): expected sign structure of the dimer-dimer correlations for the diamond-VBS state. This sign structure is used to define the order parameter O_{VBS} in Eq. (6). (b): observed ground-state dimer-dimer correlations in the VBS phase for $J_2/J_1 = -0.4$, $J_3/J_1 = -0.9$. Red (blue) corresponds to positive (negative) correlation. The black line is used as the reference bond and the grey area shows the 36-site simulation cell. (c) energy spectra with quantum numbers for $J_3 = -2$ and $S_z = 0$. Different colors and symbols denote different quantum numbers. Full (empty) symbols denote even (odd) spin-flip symmetry eigenstates. The spin-nematic phase extends up to $J_2 \lesssim -0.9$ (orange shaded region). The first excited level is a singlet with space group quantum number M.D2.A1. The diamond VBS phase exists in the window (pink shaded region) $-0.9 \gtrsim J_2 \gtrsim -0.7$. The first excited state is a singlet with space group quantum number M.D2.A2. Beyond, the $\mathbf{q} = 0$ is stabilized with triplet excitations (green shaded region). The narrow grey shaded region highlights the putative quantum critical Néel-VBS transition.

Diamond VBS phase — To identify the VBS and the lattice symmetry breaking spin-nematic phase we consider the connected dimer correlations,

$$D_{kl} \equiv \langle (\vec{S}_k \cdot \vec{S}_l)(\vec{S}_1 \cdot \vec{S}_0) \rangle - \langle \vec{S}_k \cdot \vec{S}_l \rangle \langle \vec{S}_1 \cdot \vec{S}_0 \rangle, \quad (5)$$

where the sites 0 and 1 are an arbitrary nearest-neighbor bond chosen as reference. These correlations are long-ranged in the VBS phase and exhibit specific patterns of positive and negative correlation that can be predicted for model VBS state. The sign structure of these correlations serves as a first fingerprint of the particular VBS phase realized. For the diamond VBS state the expected sign structure of the dimer correlations are shown in Fig. 3(a). Thereby, we define an order parameter of the VBS phase,

$$O_{\text{VBS}} \equiv \frac{1}{N} \sum_{\langle k,l \rangle} \theta_{kl}^{\text{VBS}} D_{kl}, \quad (6)$$

where $\theta_{kl}^{\text{VBS}} = \pm 1$ denotes the sign as defined in Fig. 3(a).

This diamond VBS parameter O_{VBS} is shown in Fig. 2(c), indicating the extent of the VBS phase. It is located between the two magnetic orders and extends basically along the whole classical critical line from $J_2 = -1$ to $J_3 = 0$. The region of pronounced O_{VBS} also coincides with the pink region in Fig. 1. There, the first excited state is a singlet $S = 0$ state with M.D2.A2 space group quantum number.

The precise nature of the reported VBS itself requires some more care. There are two basic candidate VBS model states with a twelve site unit cell [12, 31–33]. A pinwheel VBS, where all dimers are static and the pinwheels all share the same orientation. This particular state is eightfold degenerate, a factor four from the translations and a factor two from the pinwheel orientation. On the other hand, like in many other VBS scenarios, there is a resonant version of this VBS,

where we consider resonances involving eight-site loops in the shape of a diamond lozenge. A fully packed state of non-overlapping resonances is shown in Fig. 1(c). This state is actually twelve-fold degenerate, a factor four from the translations, and a factor three from the orientations of the diamond lozenges. The dimer-dimer correlations in these two model states are identical, so that dimer correlations can not distinguish the two states. However the spectral decomposition [29] reveals that beyond some common levels the diamond VBS features a characteristic spin singlet Γ .D6.E2 level, while the pinwheel VBS comes with a characteristic Γ .D6.A2 level. A close inspection of the energy spectrum of the VBS phase in Fig. 3(c) reveals a low-lying spin singlet Γ .D6.E2 level, and the absence of a low-lying Γ .D6.A2 level, thus clarifying the presence of a *diamond* VBS phase in this parameter region.

Spin nematic-plaquette phase — The dimer correlations also exhibit a different peculiar sign structure in another parameter region, as shown for $J_2 = -1$ and $J_3 = -2$ in Fig. 4(a). We see characteristic positively correlated hexagon patterns suggesting a 2×2 unit cell superstructure. However we are unaware of a *singlet* VBS model state exhibiting such a correlation pattern. We analogously define an order parameter for this lattice symmetry breaking pattern,

$$O_{\text{nem}} \equiv \frac{1}{N} \sum_{\langle k,l \rangle} \theta_{kl}^{\text{nem}} D_{kl}, \quad (7)$$

where $\theta_{kl}^{\text{nem}} = \pm 1$ is defined according to Fig. 4(c). The region in parameter space where its signal is strong is shown in Fig. 1(d).

Since we are unaware of a singlet VBS with this structure, and due to the vicinity of the ferromagnet, we explore the possibility of a phase with additional spin-nematic character, for example of quadrupolar type [34]. Several examples of frustrated ferromagnets giving rise to spin nematic phases have

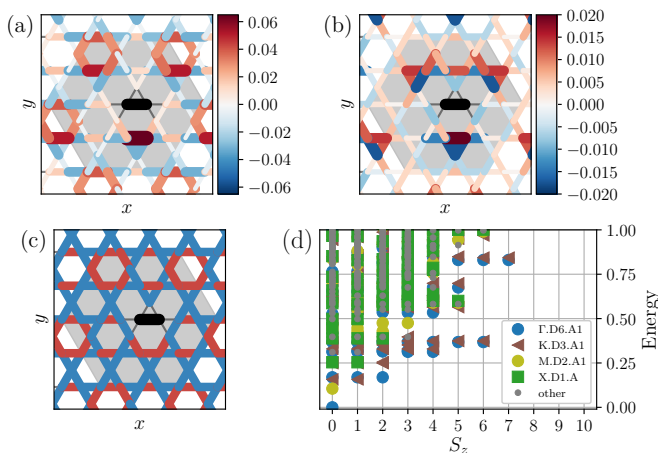


FIG. 4. Characterization of the spin nematic phase. (a): observed ground-state dimer-dimer correlations D_{kl} in the nematic phase for $J_2/J_1 = -1$, $J_3/J_1 = -2$ as defined in Eq. (5). Red (blue) corresponds to positive (negative) correlation. The black line is used as the reference bond and the grey area shows the 36-site simulation cell. (b): quadrupolar ground state correlations Q_{kl} as defined in Eq. (8) showing hexagon-ring sign structure (c): sign structure used to define nematic-dimer order parameter. Hexagons of positive correlations form a 2-by-2 unit cell. (d) Energy spectrum for $J_2 = -1$, $J_3 = -2$ in the nematic phase for $S_z < 9$. The degeneracy at different S_z gives total spin quantum number S . Odd- S sectors are not present in the low-energy tower-of-states, indicating a quadrupolar spin-nematic phase.

been discussed [35–38]. In Fig. 4(b) we display the quadrupolar bond correlations,

$$Q_{kl} \equiv \langle (S_k^+ S_l^+) (S_1^- S_0^-) \rangle, \quad (8)$$

exhibiting sizeable correlations. We notice a peculiar hexagon-ring sign structure, where the correlations on hexagons surrounding the middle hexagon are negative, while correlations on the other hexagons are positive. In Fig. 4(d) we show an energy spectrum resolved by total S^z and we can see a low-lying $S = 2$ level, which could be due to the quadrupolar character. The lowest singlet excited state is a M.D2.A1 level, which is in agreement with the reported 2×2 hexagon plaquette superstructure. So we see quite strong evidence for a novel phase, distinct from the other reported phases, but a detailed characterization of the phase has to be left for future research.

Discussion and Outlook— We have explored the appearance of two unexpected phases along the classical transition line in the $S = 1/2$ kagome Heisenberg antiferromagnet with competing ferromagnetic further neighbor couplings. The first phase is a *diamond* VBS with a twelve site unit cell. This VBS or variants thereof have been seen in quantum dimer models [11, 32, 33, 39, 40] and hinted at by fluctuations or weak correlations in quantum spin models at the nearest-neighbor point ($J_2 = J_3 = 0$) in Refs. [12, 19]. We have now firmly established this VBS phase in the extended model (1). The

location of this VBS phase in the immediate vicinity of the $\mathbf{q} = 0$ magnetic order, and the apparent second-order nature of the phase transition between the two phases in exact diagonalization, places this transition into a contender role for an example of a deconfined quantum critical transition, with possibly deconfined spin excitations at the transition [41]. Recent analytical work on the triangular lattice [42] and the analysis of the matching VBS and Néel monopoles in the Dirac spin liquid [43] combined with our numerical results renders this scenario at least plausible. It will also be important to work out the connection between the VBS phase and the Dirac spin liquid state, which is currently a prime candidate to describe the kagome antiferromagnet at small antiferromagnetic J_2 coupling [14–18], before entering the $\mathbf{q} = 0$ magnetic ordered phase.

This part of the phase diagram is then separated by a likely first order phase transition from the $\sqrt{3} \times \sqrt{3}$ magnetically ordered phase phase and the lattice symmetry breaking spin nematic phase close to the ferromagnetic phase. The precise nature of the latter phase is left for future studies.

We acknowledge useful discussions with Y.-C. He, G. Misguich, and C. Wang. The Flatiron Institute is a division of the Simons Foundation. We thank the Austrian Science Fund FWF for support within the project DFG-FOR1807 (I-2868). This research was supported in part by Perimeter Institute for Theoretical Physics. Research at Perimeter Institute is supported by the Government of Canada through the Department of Innovation, Science, and Economic Development, and by the Province of Ontario through the Ministry of Research and Innovation. The computational results presented have been achieved in part using the HPC infrastructure LEO of the University of Innsbruck. The computational results presented have been achieved in part using the Vienna Scientific Cluster (VSC).

* awietek@flatironinstitute.org

- [1] Leon Balents, “Spin liquids in frustrated magnets,” *Nature* **464**, 199–208 (2010).
- [2] Lucile Savary and Leon Balents, “Quantum spin liquids: a review,” *Reports on Progress in Physics* **80**, 016502 (2016).
- [3] Chanchal K. Majumdar and Dipan K. Ghosh, “On next-nearest-neighbor interaction in linear chain. i,” *Journal of Mathematical Physics* **10**, 1388–1398 (1969).
- [4] J.-B. Fouet, M. Mambrini, P. Sindzingre, and C. Lhuillier, “Planar pyrochlore: A valence-bond crystal,” *Phys. Rev. B* **67**, 054411 (2003).
- [5] Matthieu Mambrini, Andreas Läuchli, Didier Poilblanc, and Frédéric Mila, “Plaquette valence-bond crystal in the frustrated heisenberg quantum antiferromagnet on the square lattice,” *Phys. Rev. B* **74**, 144422 (2006).
- [6] M. E. Zhitomirsky and Kazuo Ueda, “Valence-bond crystal phase of a frustrated spin-1/2 square-lattice antiferromagnet,” *Phys. Rev. B* **54**, 9007–9010 (1996).
- [7] J. B. Marston and C. Zeng, “Spinpeierls and spinliquid phases of kagome quantum antiferromagnets,” *Journal of Applied Physics* **69**, 5962–5964 (1991).

- [8] P. W. Leung and Veit Elser, “Numerical studies of a 36-site kagome antiferromagnet,” *Phys. Rev. B* **47**, 5459–5462 (1993).
- [9] P. Nikolic and T. Senthil, “Physics of low-energy singlet states of the kagome lattice quantum heisenberg antiferromagnet,” *Phys. Rev. B* **68**, 214415 (2003).
- [10] Rajiv R. P. Singh and David A. Huse, “Ground state of the spin-1/2 kagome-lattice heisenberg antiferromagnet,” *Phys. Rev. B* **76**, 180407 (2007).
- [11] Sylvain Capponi, V. Ravi Chandra, Assa Auerbach, and Marvin Weinstein, “ p_6 chiral resonating valence bonds in the kagome antiferromagnet,” *Phys. Rev. B* **87**, 161118 (2013).
- [12] Simeng Yan, David A. Huse, and Steven R. White, “Spin-Liquid Ground State of the $S = 1/2$ Kagome Heisenberg Antiferromagnet,” *Science* **332**, 1173–1176 (2011).
- [13] Stefan Depenbrock, Ian P. McCulloch, and Ulrich Schollwöck, “Nature of the Spin-Liquid Ground State of the $S = 1/2$ Heisenberg Model on the Kagome Lattice,” *Phys. Rev. Lett.* **109**, 067201 (2012).
- [14] Ying Ran, Michael Hermele, Patrick A. Lee, and Xiao-Gang Wen, “Projected-wave-function study of the spin-1/2 heisenberg model on the kagomé lattice,” *Phys. Rev. Lett.* **98**, 117205 (2007).
- [15] Yasir Iqbal, Federico Becca, and Didier Poilblanc, “Projected wave function study of \mathbb{Z}_2 spin liquids on the kagome lattice for the spin- $\frac{1}{2}$ quantum Heisenberg antiferromagnet,” *Phys. Rev. B* **84**, 020407 (2011).
- [16] Yasir Iqbal, Federico Becca, Sandro Sorella, and Didier Poilblanc, “Gapless spin-liquid phase in the kagome spin- $\frac{1}{2}$ heisenberg antiferromagnet,” *Phys. Rev. B* **87**, 060405 (2013).
- [17] Yin-Chen He, Michael P. Zaletel, Masaki Oshikawa, and Frank Pollmann, “Signatures of dirac cones in a dmrg study of the kagome heisenberg model,” *Phys. Rev. X* **7**, 031020 (2017).
- [18] H. J. Liao, Z. Y. Xie, J. Chen, Z. Y. Liu, H. D. Xie, R. Z. Huang, B. Normand, and T. Xiang, “Gapless spin-liquid ground state in the $s = 1/2$ kagome antiferromagnet,” *Phys. Rev. Lett.* **118**, 137202 (2017).
- [19] Andreas M. Läuchli, Julien Sudan, and Roderich Moessner, “The $S = 1/2$ Kagome Heisenberg Antiferromagnet Revisited,” arXiv e-prints, arXiv:1611.06990 (2016), arXiv:1611.06990 [cond-mat.str-el].
- [20] B. Bauer, L. Cincio, B. P. Keller, M. Dolfi, G. Vidal, S. Trebst, and A. W. W. Ludwig, “Chiral spin liquid and emergent anyons in a kagome lattice mott insulator,” *Nature Communications* **5**, 5137 (2014).
- [21] Shou-Shu Gong, Wei Zhu, and D. N. Sheng, “Emergent chiral spin liquid: Fractional quantum hall effect in a kagome heisenberg model,” *Sci. Reports* **4**, 6317 (2014).
- [22] Alexander Wietek, Antoine Sterdyniak, and Andreas M. Läuchli, “Nature of chiral spin liquids on the kagome lattice,” *Phys. Rev. B* **92**, 125122 (2015).
- [23] Yin-Chen He, D. N. Sheng, and Yan Chen, “Chiral spin liquid in a frustrated anisotropic kagome heisenberg model,” *Phys. Rev. Lett.* **112**, 137202 (2014).
- [24] L. Messio, C. Lhuillier, and G. Misguich, “Lattice symmetries and regular magnetic orders in classical frustrated antiferromagnets,” *Phys. Rev. B* **83**, 184401 (2011).
- [25] Laura Messio, Bernard Bernu, and Claire Lhuillier, “Kagome antiferromagnet: A chiral topological spin liquid?” *Phys. Rev. Lett.* **108**, 207204 (2012).
- [26] B. Fåk, E. Kermarrec, L. Messio, B. Bernu, C. Lhuillier, F. Bert, P. Mendels, B. Koteswararao, F. Bouquet, J. Ollivier, A. D. Hillier, A. Amato, R. H. Colman, and A. S. Wills, “Kapellasite: A kagome quantum spin liquid with competing interactions,” *Phys. Rev. Lett.* **109**, 037208 (2012).
- [27] E. Kermarrec, A. Zorko, F. Bert, R. H. Colman, B. Koteswararao, F. Bouquet, P. Bonville, A. Hillier, A. Amato, J. van Tol, A. Ozarowski, A. S. Wills, and P. Mendels, “Spin dynamics and disorder effects in the $s = \frac{1}{2}$ kagome heisenberg spin-liquid phase of kapellasite,” *Phys. Rev. B* **90**, 205103 (2014).
- [28] Alexander Wietek and Andreas M. Läuchli, “Sublattice coding algorithm and distributed memory parallelization for large-scale exact diagonalizations of quantum many-body systems,” *Phys. Rev. E* **98**, 033309 (2018).
- [29] See the supplementary material for further information on the geometry of the lattice, its reciprocal lattice and the naming convention of the representations of the space group.
- [30] P. Lecheminant, B. Bernu, C. Lhuillier, L. Pierre, and P. Sindzingre, “Order versus disorder in the quantum heisenberg antiferromagnet on the kagomé lattice using exact spectra analysis,” *Phys. Rev. B* **56**, 2521–2529 (1997).
- [31] Didier Poilblanc and Grégoire Misguich, “Competing valence bond crystals in the kagome quantum dimer model,” *Phys. Rev. B* **84**, 214401 (2011).
- [32] Yejin Huh, Matthias Punk, and Subir Sachdev, “Vison states and confinement transitions of \mathbb{Z}_2 spin liquids on the kagome lattice,” *Phys. Rev. B* **84**, 094419 (2011).
- [33] Kyusung Hwang, Yejin Huh, and Yong Baek Kim, “ \mathbb{Z}_2 gauge theory for valence bond solids on the kagome lattice,” *Phys. Rev. B* **92**, 205131 (2015).
- [34] K. Penc and A. M. Läuchli, “Spin nematic phases in quantum spin systems,” in *Introduction to Frustrated Magnetism*, Springer Series in Solid-State Sciences, Vol. 164, edited by C. Lacroix, P. Mendels, and F. Mila (Springer, Berlin, Heidelberg, 2010) Chap. 13.
- [35] Nic Shannon, Tsutomu Momoi, and Philippe Sindzingre, “Nematic order in square lattice frustrated ferromagnets,” *Phys. Rev. Lett.* **96**, 027213 (2006).
- [36] Tsutomu Momoi, Philippe Sindzingre, and Nic Shannon, “Octupolar order in the multiple spin exchange model on a triangular lattice,” *Phys. Rev. Lett.* **97**, 257204 (2006).
- [37] Toshiya Hikihara, Lars Kecke, Tsutomu Momoi, and Akira Furusaki, “Vector chiral and multipolar orders in the spin- $\frac{1}{2}$ frustrated ferromagnetic chain in magnetic field,” *Phys. Rev. B* **78**, 144404 (2008).
- [38] Julien Sudan, Andreas Lüscher, and Andreas M. Läuchli, “Emergent multipolar spin correlations in a fluctuating spiral: The frustrated ferromagnetic spin- $\frac{1}{2}$ heisenberg chain in a magnetic field,” *Phys. Rev. B* **80**, 140402 (2009).
- [39] Zhihao Hao, Stephen Inglis, and Roger Melko, “Destroying a topological quantum bit by condensing ising vortices,” *Nature Communications* **5**, 5781 EP – (2014).
- [40] Arnaud Ralko, Frédéric Mila, and Ioannis Rousochatzakis, “Microscopic theory of the nearest-neighbor valence bond sector of the spin- $\frac{1}{2}$ kagome antiferromagnet,” *Phys. Rev. B* **97**, 104401 (2018).
- [41] T. Senthil, Ashvin Vishwanath, Leon Balents, Subir Sachdev, and Matthew P. A. Fisher, “Deconfined quantum critical points,” *Science* **303**, 1490–1494 (2004).
- [42] Chao-Ming Jian, Alex Thomson, Alex Rasmussen, Zhen Bi, and Cenke Xu, “Deconfined quantum critical point on the triangular lattice,” *Phys. Rev. B* **97**, 195115 (2018).
- [43] Xue-Yang Song, Chong Wang, Ashvin Vishwanath, and Yin-Chen He, “Unifying Description of Competing Orders in Two Dimensional Quantum Magnets,” arXiv e-prints, arXiv:1811.11186 (2018), arXiv:1811.11186 [cond-mat.str-el].
- [44] Robert S. Mulliken, “Report on notation for the spectra of polyatomic molecules,” *J. Chem. Phys.* **23**, 1997–2011 (1955).

- [45] Alexander Wietek, Michael Schuler, and Andreas M. Luchli, “Studying continuous symmetry breaking using energy level spectroscopy,” arXiv E-prints (2017), [arXiv:1704.08622](https://arxiv.org/abs/1704.08622) [[cond-mat.str-el](https://arxiv.org/archive/cond)].
- [46] Grégoire Misguich and Philippe Sindzingre, “Detecting spontaneous symmetry breaking in finite-size spectra of frustrated quantum antiferromagnets,” *Journal of Physics: Condensed Matter* **19**, 145202 (2007).

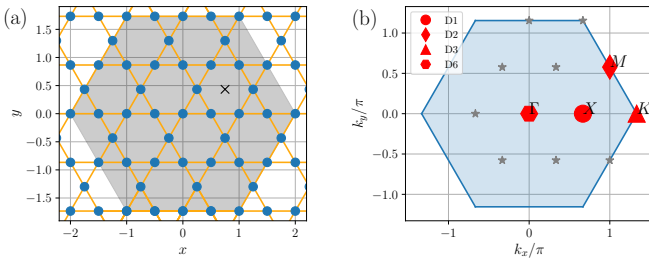


FIG. S1. (a) Kagome lattice structure and Wigner-Seitz cell of 36-site simulation cluster used. (b) Brillouin zone and reciprocal lattice of the 36-site simulation cluster. The irreducible wedge is marked by red symbols. The shape of the symbols denotes the little group of the crystal momentum.

Supplementary material to “Valence bond solid in extended kagome lattice Heisenberg antiferromagnet”

Simulation cluster geometry and symmetries

We use a 36 site kagome lattice with periodic boundary conditions shown in Fig. S1(a). The cluster features sixfold rotational symmetry and spatial reflection symmetry. In reciprocal space, it features the K and M point, cf. Fig. S1(b), which are necessary to stabilize the $\sqrt{3} \times \sqrt{3}$ magnetic order and the diamond valence bond solid (VBS) state.

We use the following naming convention when referring to irreducible representations of the space group,

$$\mathbf{q}.\mathcal{L}\mathcal{G}.\rho, \quad (\text{S1})$$

where \mathbf{q} denotes the reciprocal lattice vector, so one of Γ , X, M, K in the case of the 36 site cluster in Fig. S1. $\mathcal{L}\mathcal{G}$ denotes the little group of the crystal momentum \mathbf{q} . The names Dk ($k = 1, 2, 3, 6$) denote the dihedral groups of order $2k$, comprised of k -fold rotational symmetry plus an additional spatial reflection symmetry. ρ denotes the irreducible representation of the little group, according to the standard Mulliken naming convention introduced in Ref [44].

Exact Diagonalizations are performed in the symmetrized bases with respect to the irreducible representations of the space group. Moreover, we employ S_z conservation and the C2 spin-flip symmetry,

$$[H, F] = 0 \text{ where } F |\sigma_1, \dots, \sigma_N\rangle = |-\sigma_1, \dots, -\sigma_N\rangle. \quad (\text{S2})$$

Even (odd) spinflip symmetry sectors correspond to even (odd) total spin S , if the number of lattice sites is a multiple of 4. Details on the Exact Diagonalization method employed are explained in Ref. [28].

Ordering and tower-of-states analysis

We show the two types of magnetic ordering encountered in the main text in Fig. S2. The spin structure factor of those two

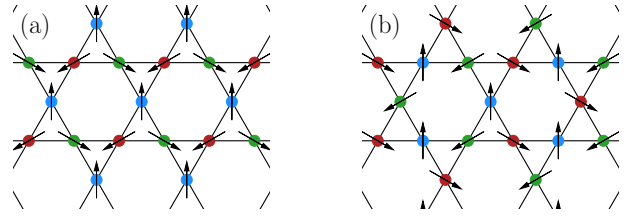


FIG. S2. Pattern of magnetic ordering for the (a) $\mathbf{q} = 0$, and (b) $\sqrt{3} \times \sqrt{3}$ phases.

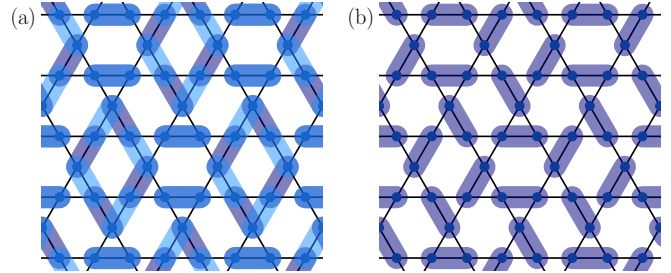


FIG. S3. (a) Diamond VBS. The two-inequivalent coverings of a “diamond” are in resonance. (b) Pinwheel VBS. Only one of the two coverings is realized. Both types of VBS can be distinguished by their respective quantum numbers.

orders is peaked at different locations in the extended Brillouin zone, cf. Ref. [24]. In the thermodynamic limit, antiferromagnetic $SU(2)$ symmetry breaking yields degenerate ground states in all total spin sectors S , which manifest itself on a finite lattice as the tower-of-states. The quantum numbers of these states can be derived analytically and compared to numerical calculations, see Ref [45]. We state the results of this derivation for the $\mathbf{q} = 0$ and $\sqrt{3} \times \sqrt{3}$ in table S1.

We considered two VBS with different pattern of valence bond configurations. The diamond VBS in Fig. S3(a) has resonant dimer patterns on the “diamond” structure, whereas the so-called pinwheel VBS realizes only one of the two states. The sign of dimer correlation patterns of both VBS are identical, and hence these two states cannot be distinguished by this order parameter. The quantum numbers of the degenerate ground states, however, are different for those two states. These quantum numbers can also be derived by investigating the representation theory of the space symmetry group acting on the VBS ansätze, cf. Refs. [45, 46]. We state the result of our derivation in table S1. The two VBS configurations can be distinguished by the appearance of a $\Gamma.D6.E2$ states in the degenerate ground state manifold, which is not present in the pinwheel VBS case.

	$\mathbf{q} = 0$ order			$\sqrt{3} \times \sqrt{3}$ order		
S	$\Gamma.D6.A1$	$\Gamma.D6.A2$	$\Gamma.D6.E2$	$\Gamma.D6.A1$	$\Gamma.D6.B1$	$K.D3.A1$
0	1	0	0	1	0	0
1	0	1	1	0	1	1
2	1	0	2	1	0	2
3	1	2	2	1	2	2
Diamond VBS ($S = 0$): $\Gamma.D6.A1, \Gamma.D6.A2, 2 \times \Gamma.D6.E2, M.D2.A1, M.D2.A2$						
Pinwheel VBS ($S = 0$): $\Gamma.D6.A1, \Gamma.D6.A2, M.D2.A1, M.D2.A2$						

TABLE S1. Quantum numbers constituting the tower-of-states of the $\mathbf{q} = 0$ and $\sqrt{3} \times \sqrt{3}$ magnetic ordering and quantum numbers of the degenerate $S = 0$ states of the pinwheel and diamond VBS state.